Variable Temperature LED-NMR: Rapid Insights Into a Photocatalytic Mechanism from Reaction Progress Kinetic Analysis

Wesley B. Swords, 1 Steven J. Chapman, 1 Heike Hofstetter, 1 Anna L. Dunn, 21* Tehshik P. Yoon 1*

¹Department of Chemistry, University of Wisconsin-Madison, Madison, Wisconsin 53703, USA.

ABSTRACT: A multitude of techniques are available to obtain a useful understanding of photocatalytic mechanisms. The combination of LED illumination with nuclear magnetic resonance spectroscopy (LED–NMR) provides a rapid, convenient means to directly monitor a photocatalytic reaction in situ. Herein, we describe a study of the mechanism of an enantioselective intermolecular [2+2] photocycloaddition catalyzed by a chiral Ir photocatalyst using LED–NMR. The data-rich output of this experiment is suitable for same excess and variable time normalization analyses (VTNA). Together, these identified an unexpected change in mechanism between reactions conducted at ambient and cryogenic temperatures. At -78 °C, the kinetic data are consistent with the triplet rebound mechanism we previously proposed for this reaction, involving sensitization of maleimide and rapid reaction with a hydrogen-bound quinoline within the solvent cage. At room temperature, the cycloaddition instead proceeds through intracomplex energy transfer to the hydrogen-bound quinolone. These results highlight the potential sensitivity of photocatalytic reaction mechanisms to the precise reaction conditions and the further utility of LED–NMR as a fast, data-rich tool for their interrogation that compares favorably to conventional ex situ kinetic analyses.

INTRODUCTION

Photocatalysis continues to attract the interests of synthetic chemists in both academic and industrial contexts. Photocatalytic reactions provide facile access to highly reactive species under mild conditions and can enable distinctive reactivity that is not otherwise accessible under thermal conditions. The continued development and optimization of photocatalytic reactions requires a detailed understanding of photochemical mechanisms. Moreover, as photocatalytic techniques become increasingly adopted by the pharmaceutical industry,1 determination of the rate laws and reaction profiles for these processes is becoming an increasingly critical concern for safe and reproducible scale-up.² Presently, the macroscopic reaction rate law of a photochemical reaction is typically determined using time-intensive ex situ initial rate measurements. As Blackmond, Burés, and others have previously argued, such initial rate experiments are information-poor: they typically involve the collection of a single data point at low conversion, and aggregate analysis of multiple initial rate measurements is required to determine a complete rate law.3 Moreover, important effects that might occur after the initial rate regime, such as product inhibition, intermediate formation, and catalyst degradation, can be obscured using initial-rate data, restricting a holistic understanding of a complex catalytic reaction mechanism.

In the study of ground-state catalytic reactions, operando techniques such as NMR, IR, UV-Vis, and calorimetry have emerged as powerful tools for reaction mechanism determination. NMR, in particular, provides access to structural information and the ability to detect and identify intermediates and byproducts along with data useful for kinetic analyses. The resulting complete reaction profiles are information-rich and amenable to modern kinetic graphical analyses that avoid the need for time-intensive ex situ measurements. The concept of reaction progress kinetic analysis (RPKA) was

formalized by Blackmond as a mechanistic tool for the study of complex catalytic reactions.^{3a,4} In 2016 Burés expanded this concept by developing variable time normalization analysis (VTNA), which uses the graphical representation of multiple kinetic experiments to visually determine substrate and catalyst reaction orders.^{5,6} Together, these techniques enable a holistic understanding of a catalytic reaction mechanism from only a few data-rich time course experiments. While their impact on the study of ground-state catalytic reactions has grown significantly in the past two decades, these techniques have only been sparingly applied to photocatalytic reactions to date.⁷

One powerful strategy to collect information-rich photochemical reaction progress data was pioneered by Gschwind,8 who demonstrated that photocatalytic reactions can be monitored in situ by directing light from a high-powered light emitting diode (LED) through fiber optic cabling into the bore of an NMR spectrometer.9 The Gschwind group has applied the LED-NMR technique to study several photocatalytic redox transformations and ligand exchange reactions. 10 Our group found that LED-NMR experiments have the resolution to monitor very fast photocatalytic reactions that reach full conversion in <2 min, 11 while Riedle has applied the technique to the modeling of molecular motors at cryogenic temperatures.¹² Merck has used LED-NMR in the development of photocatalytic reactions¹³ and to rapidly determine reaction quantum yields, ¹⁴ while AstraZeneca used it in the development of a large-scale photoredox Minisci reaction.¹⁵ Thus, LED-NMR is emerging as a powerful technique for studying the kinetics of a variety of photochemical processes in both academic and industrial contexts.

Our group has a long-standing interest in the development of asymmetric photocatalytic reactions and in the interrogation of their mechanisms. We recently reported a highly enantioselective photocatalytic [2+2] cycloaddition between quinolone ${\bf Q}$ and maleimide

²Pharmaceutical Development, GlaxoSmithKline, Upper Providence, Pennsylvania 19426, USA.

M. Upon visible light irradiation at -78 °C in the presence of chiral iridium complex Ir, cycloadduct P is produced in good yield and in 97% ee (Scheme 1).16 Interestingly, a combination of kinetic, spectroscopic, and computational evidence suggested that the reaction proceeds through an unusual "triplet rebound" mechanism (Scheme 1). NMR spectroscopy revealed that the chiral Ir catalyst and Q preassociate in the ground state through a discrete hydrogenbond interaction ([Ir-Q], $K_{EQ} = 603$). Photoexcitation of this ground-state complex results in a long-lived luminescent excited state [3Ir-Q]. We found that intracomplex energy transfer from 3Ir to bound **Q** is significantly slower than intermolecular energy transfer to M. This was a surprising finding. It indicated that reaction of the excited-state maleimide within a solvent caged ternary encounter complex $\{[Ir-Q]^{--3}M\}$ must be the dominant product-forming pathway in order to account for the observed high ee's at low catalyst loadings. The mechanism of this reaction intrigued us because it represents a departure from all previous approaches to asymmetric catalysis of excited-state photoreactions, which require the excited state intermediate to be generated within a preassociated complex with a chiral catalyst.17

Scheme 1. Asymmetric Photosensitized Cycloaddition and Proposed Reaction Mechanism.

We wondered if in situ LED–NMR might provide a means to rapidly collect kinetic data to deepen our understanding of this reaction. In particular, we imagined that RPKA analysis could provide insight into the possibility of unproductive processes such as product inhibition and maleimide dimerization that might be difficult to investigate using conventional initial rate experiments. Miller has recently used LED–NMR in a VTNA analysis of a photoinduced transfer hydrogenation reaction. ¹⁸ However, no applications of VTNA to stereocontrolled photocatalysis have yet been reported.

Herein we show that LED–NMR enables the use of VTNA to interrogate the enantioselective intermolecular [2+2] photocycloaddition at different temperatures. These studies revealed a significant change in reaction mechanism between 24 to $-78\,^{\circ}$ C. We find that the triplet rebound reaction is favored at cold temperatures, while intracomplex energy transfer to hydrogen bound quinolone is favored at 24 $^{\circ}$ C. The rate laws determined by VTNA were verified with initial rate measurements that proved to be significantly more laborious to complete. Thus, these results show how powerful the

LED-NMR technique can be in the study complex photocatalytic mechanisms that can be highly sensitive to the precise reaction conditions

RESULTS AND DISCUSSION

The design of the LED-NMR system at UW-Madison was inspired by Gschwind¹² and has been detailed by us previously.¹¹ Briefly, light from an ultra-high-powered (UHP) 450 nm LED is directed via an optical fiber inserted within the 5 mm NMR tube containing the sample. The tip of the optical fiber is placed such that irradiation occurs from the top of the detection coil. This set-up is flexible and mobile; in this study, NMR spectra were collected on 600 and 500 MHz spectrometers for 24 °C and -78 °C measurements, respectively. Our study began by determining the optimal light intensity for the standard reaction, with the goal that the reaction would reach near completion (>90% conversion of \mathbf{Q}) within ~ 1 h. This was achieved with an LED power of 300 mW at 24 °C under otherwise identical conditions to those reported previously (0.02 M Q, 5 equiv. M, and 1.5 mol% Ir in CD₂Cl₂). Time course data were collected as single 1H spectra every 20 s with a pseudo-2D pulse program (SI). An example of the collected NMR spectra and plotted time-course for the parent reaction under standard conditions are shown in Figure 1.

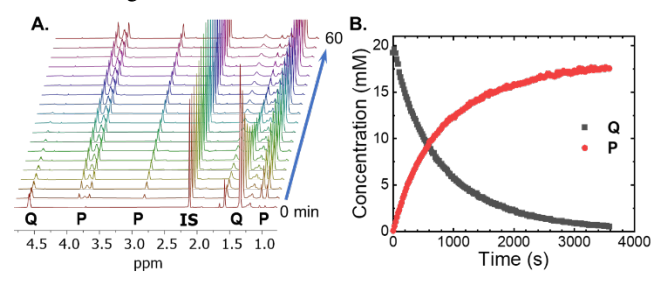


Figure 1. A. NMR spectra for the standard reaction: 300 mW 450 nm LED, 0.02 M \mathbf{Q} , 1.5 equiv. \mathbf{M} , 1.5 mol% \mathbf{Ir} , CD₂Cl₂. Spectra were collected every 20s for 1 h, every tenth spectrum is shown, hexamethylbenzene was used as an internal standard (**IS**). **B.** Reaction profile tracking the conversion of quinolone \mathbf{Q} and formation of cyclobutane \mathbf{P} .

Quinolone Q and cyclobutane P feature the same amide motif that facilitates hydrogen bond formation with the chiral catalyst. Thus, we first investigated whether product inhibition may occur in this reaction through same excess experiments. We compared the reaction profile of substrate conversion under standard conditions to a profile starting with half the concentration of **Q** (Figure 2A, 0.01 MQ). A small deviation between the two sets of data was clear when the 0.01 M Q data was time adjusted to align with the standard conditions. This suggested either photocatalyst degradation or product inhibition. To differentiate these, measurements under 50% conversion conditions including the addition of 50% enantioenriched product (produced from the Δ -Ir catalyst, ~0.01 M P, 96% ee) were performed with either the matching chiral Δ -Ir catalyst or the mismatched Λ -Ir (Figure 2B). Product inhibition was most significant under matched conditions, with the chiral product favored by the Δ -Ir catalyst. No inhibition was observable under mismatched conditions, which resulted in data superimposable with the 0.01 M Q data (Figure 2B inset). We therefore conclude that product inhibition does indeed occur in this reaction and that the major enantiomer exerts a more pronounced inhibitory effect. Notably, the four reaction profiles required for this analysis were set up and collected in just half a day.

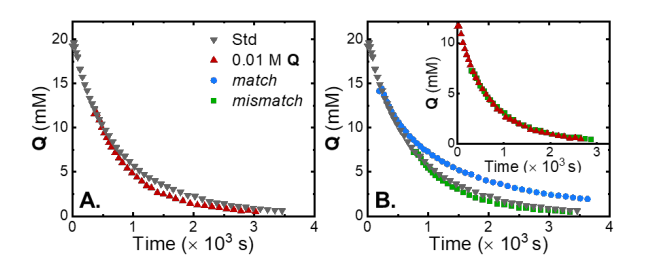


Figure 2. A. Same excess comparison between standard conditions and conditions approximating 40% reaction conversion (with no Pdt added). **B.** Same excess experiments comparing standard conditions to conditions approximating 30–50% conversion with the addition of the expected concentration of cyclobutane product; blue circles = matched **Ir** and product chirality, green squares = mismatched **Ir** and product chirality. Not all data points are shown for clarity, full data is presented in the SI.

We next sought to determine the rate law of the photocatalytic reaction using LED–NMR-enabled VTNA. For this analysis, reaction profiles are collected under conditions where the concentration of a single reaction partner is significantly altered. The time axis is replaced with the time integral of the concentration of the reagent of interest ($\bf A$) taken to a power (a), thereby normalizing the time between pairs of data points and removing the kinetic effect of $\bf A$ (eq 1).

$$\int_{t=0}^{t=n} [A]^a dt = \sum_{i=1}^n \left(\frac{[A]_i - [A]_{i-1}}{2} \right)^a (t_i - t_{i-1})$$
 (1)

The value of 'a' where the plots overlay provides the reaction order in **A**. Repeating this process for all reagents and catalysts provides the full rate law. Importantly, only a few experiments are required for this analysis, significantly reducing the number of reactions required to determine the rate law compared with ex situ initial rate experiments: the data presented in **Figure 3A–3D** was collected and analyzed in a single day.

The interpretation of the VTNA data was clear. Comparing reaction profiles collected at 0.01, 0.02, and 0.04 M quinolone indicated a first-order dependence in Q (Figure 3A). Similar analyses provided a zero-order dependence with respect to the Ir photocatalyst (Figure 3C). A benefit of the LED–NMR system is that the power of the LED is directly proportional to the intensity at the sample. The reaction rate dependence of light was interrogated at three LED powers, 150 mW, 300 mW, and 560 mW. Treating light power as a constant concentration provided a first-order dependence on LED power (Figure 3D). Finally, the dependence on maleimide was interrogated; however, due to low solubility of maleimide and its dimer, it was difficult to interpret the reaction order by VTNA. We overcame this using N-benzylmaleimide (M2), which is fully soluble under the reaction conditions and provides similar preparative results. 16 A zero-order rate dependence on M2 was observed (Figure 3B).

From these experiments we formulated the rate law for this reaction, $rate = k[Q]^1[M]^0[Ir]^0(hv)^1$. As this is one of the first uses of LED–NMR kinetic data for VTNA analysis we confirmed the reaction orders for **Q**, **M**, and **Ir** using in triplicate initial rates analysis (**Figure 4A–C**). Notably, the acquisition of the initial rate data required three days to complete, compared to the single day required for the VTNA analysis. Gratefully, the reaction orders align well with those determined using VTNA, confirming a first-order dependence on **Q** and a zero-order dependence on **M**. Interestingly, rather than

a linear dependence on **Ir**, saturation kinetics were observed. At higher concentrations of **Ir** the reaction has a zero-order dependence on **Ir**. This zero-order region is frequently called the photon-limited region, where the rate of the reaction is limited solely by the intensity of incident irradiation and not photocatalyst concentration. As the concentration of **Ir** is decreased, the reaction moves out of the photon-limited region and a dependence of the rate on **Ir** concentration becomes apparent. To model this relationship, we applied **eq 2**, which describes the expected photocatalyst saturation kinetics, where k_0 is the zeroth-order rate constant at saturation and the saturation curve is defined by the pathlength and photocatalyst extinction coefficient (b and ε , respectively).¹⁴

$$rate = k_0(1 - 10^{-\varepsilon b[Ir]}) \tag{2}$$

For the LED–NMR VTNA experiments, the pathlength within the NMR tube is ~3 cm. This, combined with a photocatalyst extinction coefficient of $1200 \, \text{M}^{-1} \, \text{cm}^{-1} \, (450 \, \text{nm})$, provides a solution to **eq** 2 of *rate* = $k_0(0.92)$ for 20 mM **Q**, placing the VTNA analysis near or within the zero-order photon-limited region.

While we were pleased to have validated the ability of LED–NMR and VTNA to rapidly acquire a reaction rate law, we were surprised to observe that these results differ significantly from those we had reported in our initial publication. In that study, we had determined the rate law as $rate=k[Q]^0[M]^1[Ir]^{1.16}$ There are three differences between these studies that we imagined might be responsible for the differences in observed rate law: some feature of the LED–NMR instrument itself, the identity of the maleimide partner (maleimide vs N-benzylmaleimide), or the reaction temperature (-78 °C in the initial publication and ambient temperature here). To investigate these possibilities, we collected in situ LED–NMR kinetic data at -75 °C using M2 in place of M. We ran experiments similar to those at rt, though with only a single variation in concentration to highlight the simplicity of VTNA combined with LED–NMR. **Figure 3E–H**

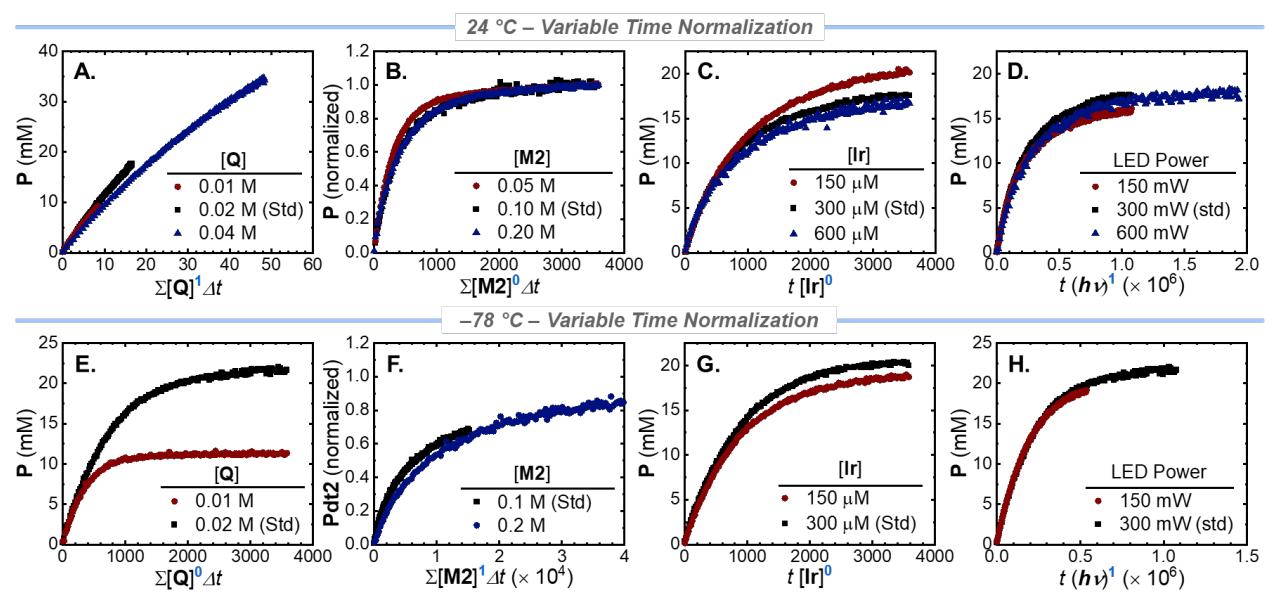


Figure 3. A–D. Variable time normalization analysis for $\mathbf{Q}(\mathbf{A})$, $\mathbf{M2}(\mathbf{B})$, $\mathbf{Ir}(\mathbf{C})$, and light (\mathbf{D}) conducted at 24 °C. E–H. Variable time normalization analysis for $\mathbf{Q}(\mathbf{E})$, $\mathbf{M2}(\mathbf{F})$, $\mathbf{Ir}(\mathbf{G})$, and light (\mathbf{H}) conducted at -78 °C. The $\mathbf{M2}$ data was normalized to starting quinolone concentration due to small changes in starting concentrations (\mathbf{B}/\mathbf{F}) , see SI for raw data). Concentration of \mathbf{Q} , $\mathbf{M2}$, and \mathbf{Ir} are noted for the different conditions studied, unless noted the other reagents were maintained at standard conditions.

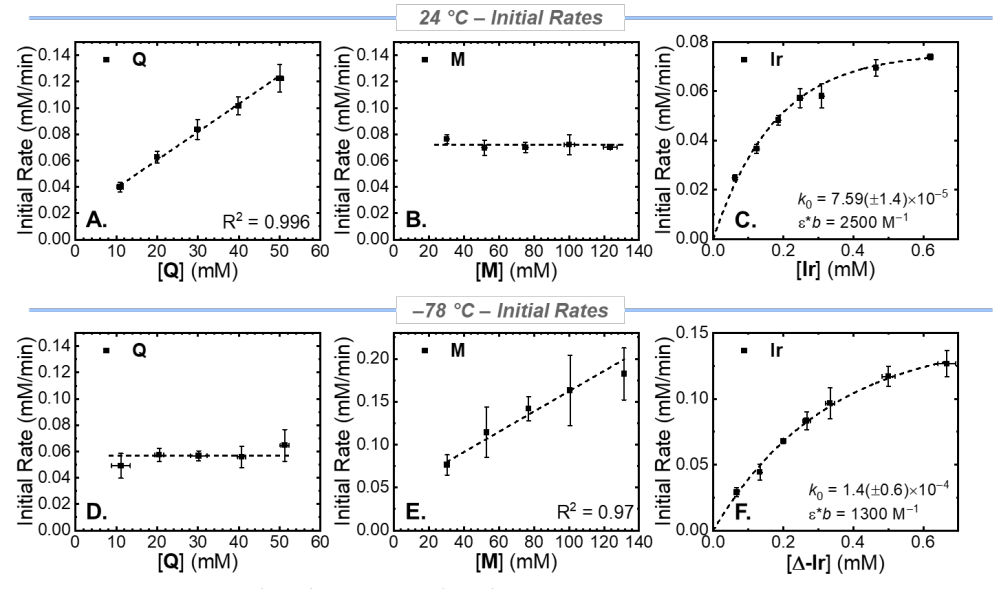


Figure 4. Ex situ initial rates collected at $24 \, (\mathbf{A} - \mathbf{C})$ and $-78 \, ^{\circ}\mathrm{C} \, (\mathbf{D} - \mathbf{F})$. Error bars are the average of three trials and, in some instances, smaller than the data point. Dotted lines correspond to a linear regression $(\mathbf{A} \text{ and } \mathbf{E})$, a fit to $\mathbf{eq} \, \mathbf{2} \, (\mathbf{C} \text{ and } \mathbf{F})$, or are drawn to guide the eye $(\mathbf{B} \text{ and } \mathbf{D})$.

shows the results of the VTNA, which indicate a rate law $rate=k[\mathbf{Q}]^0[\mathbf{M}]^1[\mathbf{Ir}]^0(hv)^1$. Notably, the reaction order with respect to \mathbf{Ir} and light are maintained between rt and -78 °C, whereas \mathbf{Q} changes to zero-order while maleimide became first-order. The deviation of the 0.1 M experimental data around 500 s in Fig 3E occurs due to depletion of the limiting reagent (\mathbf{Q}). The 0.2 M experiment with double the concentration of \mathbf{Q} requires more time to reach full conversion. The zero-order dependence on \mathbf{Q} was assigned from the complete overlap of the two reaction profiles until the 0.1 M experiment reached completion. Again, we confirmed these data with arduous initial rates experiments, which involved a full week of experimentation (see SI) rather than the single day of LED–NMR data collection. The larger error bar observed in **Figure 4E** highlights another advantage of the simplicity and consistency provided by LED–

NMR. Compared with LED–NMR, the reaction set-up (including temperature, distance from the LED, ice buildup, etc.) required to collect cryogenic ex situ initial rates is difficult to keep completely consistent across the experiments, resulting in larger errors. The LED–NMR and VTNA avoid these problems as the set-up is highly controlled with minimal variation between experiments.

In our initial disclosure of this asymmetric photocatalytic cycloaddition, density functional theory (DFT) calculations and time-resolved spectroscopy supported the bimolecular sensitization of free maleimide instead of the hydrogen-bond quinolone at cold temperatures. Our proposed triplet rebound mechanism rationalizes the preliminary initial rates measurements that gave a first-order dependence on maleimide and **Ir** and zero-order dependence on **Q** if

Scheme 2. Gibbs Free Energy Difference Between DFT Optimized Binding Geometries. Rate Determining Steps at 24 and -78 °C.

the rate-determining step at -78 °C is energy transfer from the saturated [3 **Ir**- \mathbf{Q}] complex to maleimide. We were pleased to observe that the VTNA experiment aligned well with the quinolone and maleimide reaction orders previously reported, suggesting that \mathbf{M} and $\mathbf{M2}$ play substantially similar roles in the mechanism. The discrepancy in the order in photocatalyst between in situ LED-NMR and previous probe-scale initial rates 16 can be rationalized by the different irradiation sources used (450 nm for VTNA, vs. 450–490 nm for prior initial rates). A simple Beer's law analysis indicates the light source and path length used for the LED–NMR conditions give kinetics within the photon limited region, explaining the zero-order dependence observed here.

The unexpected difference between the rate laws determined at $24~^{\circ}$ C and $-78~^{\circ}$ C was more difficult to rationalize, as it implied a change in catalytic mechanism at different temperatures. Understanding this discrepancy could provide insight into the nature of the triplet rebound mechanism and inform future efforts to optimize asymmetric photoreactions.

We previously reported the equilibrium constant for binding of **Ir** and **Q** to be $K_{\text{EQ,RT}} = 603$ at ambient temperature. This value implies that only ~85% of the Ir catalyst is bound by **Q** at 0.01 M versus 95% at 0.04 M. Conversely, time-resolved studies at $-78\,^{\circ}\text{C}$ allowed us to calculate an estimated binding constant of $K_{\text{EQ,-78}} = 3400$, which is an order of magnitude larger and corresponds to >97% bound iridium at both initial **Q** concentrations. In addition to this distinct change in binding, the change in the rate of quenching of ${}^{3}\textbf{Ir}$ by **Q** also shows a temperature dependence. At ambient temperature, steady-state luminescence quenching experiments gave a Stern–Volmer constant ($K_{\text{SV,RT}}$) of 47 M⁻¹, indicating a moderate rate of quenching of the photocatalyst by **Q**. At $-78\,^{\circ}\text{C}$, however, time-resolved lifetime measurements gave no evidence of energy transfer between **Ir** and **Q**.

These data can be interpreted in the context of the DFT models for catalyst–substrate binding we had previously reported. The calculated lowest energy conformation places the quinolone in an orientation with minimal orbital overlap with the cyclometallating ligand. We had invoked this binding model to rationalize the lack of observed energy transfer within the catalyst–substrate complex at – 78 °C. These computations, however, also identified three alternate binding geometries within 4 kcal/mol of the lowest-energy structure, some of which feature extensive overlap between the catalyst and quinolone orbitals (**Scheme 2A**). At ambient temperature, therefore, thermal motion could allow the bound quinolone to populate geometries that would permit intra-complex energy transfer.

Thus, a reasonable interpretation of these data is that the mechanism of asymmetric product formation varies as a function of temperature. At -78 °C, the photocatalyst strongly binds **Q** but holds it in a pose that precludes intracomplex energy transfer (Scheme 2C). The rate of bimolecular quenching by M is rate-determining, resulting in a first-order dependence in [M] and [Ir], and the high ee's observed imply that M must react with the [Ir-Q] complex rather than free Q in solution, consistent with the observed zero-order dependence in Q. At room temperature, thermal population of an alternate, higher-energy [Ir-Q] binding geometry enables rate-determining intracomplex energy-transfer followed by cycloaddition with M, explaining the zero-order dependence on [M] (Scheme 2B). In this scenario, the first-order dependence on Q would arise from its relatively weak association to the photocatalyst, as increased Q concentration increases the concentration of the photoactive complex. The reaction is photon-limited, and therefore the photocatalyst concentration had no effect on the rate.

We draw two important conclusions from this study. The first is that the highly enantioselective triplet rebound mechanism predominates in this system only at low temperatures where the photocatalyst-quinolone complex is relatively rigid. At higher temperatures, a more conventional intracomplex energy transfer activation step dominates. This insight may help to guide the development of future asymmetric photoreactions that rationally exploit this novel mechanism as a design strategy. Second, the mechanisms of photocatalytic reactions can be surprisingly sensitive to reaction conditions. In order to safely incorporate new photocatalytic methods into industrial-scale processes, it will become increasingly important to understand their detailed kinetic behavior, despite the many challenges in probing the mechanisms of photocatalytic reactions. These studies show that application of VTNA analysis to LED-NMR data provides a rapid and operationally facile alternative to conventional initial rate kinetic analysis that could accelerate use of this important tool in photocatalytic reaction analysis.

CONCLUSION

The data acquired from LED–NMR experiments are information-rich and amenable modern kinetic analysis techniques such as same excess experiments and VTNA. These techniques were used to interrogate the mechanism of a model asymmetric photochemical [2+2] cycloaddition at room temperature and –78 °C. We confirmed the VTNA analysis through time-consuming ex situ initial rates experiments, highlighting the ability of the LED–NMR technique to streamline kinetic analysis. VTNA experiments were able to easily identify a change in the catalytic mechanism. LED–NMR spectroscopy should thus be considered an enabling tool in

photochemical synthesis that can provide important insights into photocatalytic mechanism that could be used in the design of future asymmetric photoreactions.

ASSOCIATED CONTENT

Supporting Information

The Supporting Information is available free of charge on the ACS Publications website.

Description of LED-NMR, materials, and methods. ¹H NMR data acquisition and analysis. Batch reactions. In-triplicate initial rates measurements, same excess experiments, and VTNA experimental procedures and data. (PDF)

AUTHOR INFORMATION

Corresponding Authors

- * Anna L. Dunn: anna.dunn@merck.com
- * Tehshik P. Yoon: tyoon@chem.wisc.edu
- ¹ (a) Douglas, J. J.; Sevrin, M. J.; Stephenson, C. R. J. Visible Light Photocatalysis: Applications and New Disconnections in the Synthesis of Pharmaceutical Agents. *Org. Process Res. Dev.* **2016**, *20*, 1134–1147. (b) Mennen, S. M.; Alhambra, C.; Allen, C. L.; Barberis, M.; Berritt, S.; Brandt, T. A.; Campbell, A. D.; Castañón, J.; Cherney, A. H.; Christensen, M.; et. al. The Evolution of High-Throughput Experimentation in Pharmaceutical Development and Perspectives on the Future. *Org. Process Res. Dev.* **2019**, *23*, 1213–1242. (c) Buglioni, L.; Raymenants, F.; Slattery, A.; Zondag, S. D. A; Noël, T. Technological Innovations in Photochemistry for Organic Synthesis: Flow Chemistry, High-Throughput Experimentation, Scale-up, and Photoelectrochemistry. *Chem. Rev.* **2021**, *122*, 2752–2906. (d) Politano, F.; Oksdath-Mansilla, G. Light on the Horizon: Current Research and Future Perspectives in Flow Photochemistry. *Org. Process Res. Dev.* **2018**, *22*, 1045–1062.
- ² (a) Sezen-Edmonds, M.; Tabora, J. E.; Cohen, B. M.; Zaretsky, S.; Simmons, E. M.; Sherwood, T. C.; Ramirez, A. Predicting Performance of Photochemical Transformations for Scaling Up in Different Platforms by Combining High-Throughput Experimentation with Computational Modeling. Org. Process Res. Dev. 2020, 24, 2128–2138. (b) Chaudhuri, A.; Zondag, S. D. A.; Schuurmans, J. H. A.; Schaaf, J. v. d.; Noël, T. Scale-Up of a Heterogeneous Photocatalytic Degradation Using a Photochemical Rotor–Stator Spinning Disk Reactor. Org. Process Res. Dev. 2022, 26, 1279–1288. (c) Bonfield, H. E.; Lévesque, F.; Moschetta, E. G.; Susanne, F.; Edwards, L. J. Photons as a 21st century reagent. Nat. Comm. 2020, 11, 804. (d) Williams, J. D.; Kappe, C. O. Recent advances toward sustainable flow photochemistry. Curr. Opin. Green Sust. Chem. 2020, 10, 100351.
- ³ (a) Blackmond, D. G. Reaction Progress Kinetic Analysis: A Powerful Methodology for Mechanistic Studies of Complex Catalytic Reactions. *Angew. Chem. Int. Ed.* **2005**, *44*, 4302–4320. (b) Nielsen, C. D.-T.; Burés, J. Visual Kinetic Analysis. *Chem. Sci.* **2019**, *10*, 348–353.
- ⁴ Blackmond, D. G. Kinetic Profiling of Catalytic Organic Reactions as a Mechanistic Tool. *J. Am. Chem. Soc.* **2015**, *137*, 10852–10866.
- ⁵ Burés, J. A Simple Graphical Method to Determine the Order in Catalyst. *Angew. Chem. Int. Ed.* **2016**, *55*, 2028–2031.
- ⁶ Burés, J. Variable Time Normalization Analysis: General Graphical Elucidation of Reaction Orders from Concentration Profiles. *Angew. Chem. Int. Ed.* **2016**, *55*, 16084–16087.
- 7 (a) Malik, J. A.; Madani, A.; Pieber, B.; Seeberger, P. H. Evidence for Photocatalyst Involvement in Oxidative Additions of

Nickel-Catalyzed Carboxylate O-Arylations. J. Am. Chem. Soc. 2020, 142, 11042–11049. (b) Askey, H. E.; Grayson, J. D.; Tibbetts, J. D.; Turner-Dore, J. C.; Holmes, J. M.; Kociok-Kohn, G.; Wrigley, G. L.; Cresswell, A. J. Photocatalytic Hydroaminoalkylation of Styrenes with Unprotected Primary Alkylamines. J. Am. Chem. Soc. 2021, 143, 15936–15945. (c) Liu, W.; Lavagnino, M. N.; Gould, C. A.; Alcázar, J.; MacMillan, D. W. C. A biomimetic

Present Addresses

+ALD: Small Molecule Analytical Research & Development, Merck, Rahway, New Jersey, 07065.

ACKNOWLEDGMENT

We thank Prof. Silvia Cavagnero for the resources of the UW–Madison Center for Laser-Assisted NMR facility. Funding for this work was provided by the NSF (CHE-1954262). W.B.S. acknowledges an NIH post-doctoral fellowship (F32GM134611). The Bruker Avance III 600 NMR spectrometer and LED components were supported by NIH grant S10 OD012245. The Bruker Avance Neo 500 NMR spectrometer was supported by NSF grant CHE-2017891.

REFERENCES

S_H2 cross-coupling mechanism for quaternary sp³-carbon formation. *Science* **2021**, *374*, 1258–1263. (d) Lehnherr, D.; Ji, Y.; Neel, A. J.; Cohen, R.D.; Brunskill, A. P. J.; Yang, J; Reibarkh, M. Discovery of a Photoinduced Dark Catalytic Cycle Using in Situ LED-NMR Spectroscopy. *J. Am. Chem. Soc.* **2018**, *140*, 13843–13853.

- ⁸ Feldmeier, C.; Bartling, H.; Riedle, E.; Gschwind, R. M. LED based NMR illumination device for mechanistic studies on photochemical reactions Versatile and simple, yet surprisingly powerful. *J. Mag. Res.* **2013**, 232, 39–44.
- ⁹ (a) Nitschke, P.; Lokesh, N.; Gschwind, R. M. Combination of illumination and high resolution NMR spectroscopy: Key features and practical aspects, photochemical applications, and new concepts. *Prog. Nucl. Magn. Reson. Spectrosc.* **2019**, 114–115, 86–134. (b) Ji, Y.; DiRocco, D. A.; Kind, J.; Thiele, C. M.; Gschwind, R. M.; Reibarkh, M. LED-Illuminated NMR Spectroscopy: A Practical Tool for Mechanistic Studies of Photochemical Reactions. *ChemPhotoChem* **2019**, 3, 984–992.
- 10 (a) Feldmeier, C.; Bartling, H.; Magerl, K.; Gschwind, R. M. LEDilluminated NMR studies of flavin-catalyzed photooxidations reveal solvent control of the electron-transfer mechanism. Angew. Chem. Int. Ed. 2015, 54, 1347-1351. (b) Petzold, D.; Nitschke, P.; Brandl, F.; Scheidler, V.; Dick, B.; Gschwind, R. M.; König, B. Visible-Light-Mediated Liberation and In Situ Conversion of Fluorophosgene. Chem. - A Eur. J. 2019, 25, 361-366. (c) Bartling, H.; Eisenhofer, A.; Konig, B.; Gschwind, R. M. The Photocatalyzed Aza-Henry Reaction of N-Aryltetrahydroisoquinolines: Comprehensive Mechanism, H*- versus H*-Abstraction, and Background Reactions. J. Am. Chem. Soc. 2016, 138, 11860-11871. (d) Chen, K.; Berg, N.; Gschwind, R.; König, B. Selective Single C(sp3)-F Bond Cleavage in Trifluoromethylarenes: Merging Visible-Light Catalysis with Lewis Acid Activation. J. Am. Chem. Soc. 2017, 139, 18444-18447. (e) Wang, S.; Lokesh, N.; Hioe, J.; Gschwind, R. M.; König, B. Photoinitiated carbonyl-metathesis: deoxygenative reductive olefination of aromatic aldehydes via photoredox catalysis. Chem. Sci. 2019, 10, 4580-4587.
- ¹¹ Skubi, K. L.; Swords, W. B.; Hofstetter, H.; Yoon, T. P. LED-NMR Monitoring of an Enantioselective Catalytic [2+2] Photocycloaddition. *ChemPhotoChem* **2020**, *4*, 685–690.
- ¹² Wilcken, R.; Gerwien, A.; Huber, L. A.; Dube, H.; Riedle, E. Quantitative *In-Situ* NMR Illumination for Excitation and Kinetic Analysis of Molecular Motor Intermediates. *ChemPhotoChem.* **2022**. 6, e20210023.
- ¹³ (a) Schultz, D. M.; Levesque, F.; DiRocco, D. A.; Reibarkh, M.; Ji, Y.; Joyce, L. A.; Dropinski, J. F.; Sheng, H.; Sherry, B. D.; Davies, I. W. Oxyfunctionalization of the Remote C–H Bonds of Aliphatic Amines by Decatungstate Photocatalysis. *Angew. Chem. Int. Ed.* **2017**, *56*, 15274–15278. (b) Lehnherr, D.; Ji, Y.; Neel, A. J.; Cohen, R. D.; Brunskill, A. P. J.; Yang, J.;

Reibarkh, M. Discovery of a Photoinduced Dark Catalytic Cycle Using in Situ LED-NMR Spectroscopy. *J. Am. Chem. Soc.* **2018**, *140*, 13843–13853. (c) Ji, Y.; Bottecchia, C.; Lévesque, F.; Narsimhan, K.; Lehnherr, D.; McMullen, J. P.; Dalby, S. M.; Xiao, K.-J.; Reibarkh, M. Benzylic Photobromination for the Synthesis of Belzutifan: Elucidation of Reaction Mechanisms Using In Situ LED-NMR. *J. Org. Chem.* **2022**, *87*, 2055–2062. (d) Woo, J.; Christian, A. H.; Burgess, S. A.; Jiang, Y.; Mansoor, U. F.; Levin, M. D. Scaffold hopping by net photochemical carbondeletion of azaarenes. *Science.* **2022**, *376*, 527–532.

¹⁴ (a) Ji, Y.; DiRocco, D. A.; Hong, C. M.; Wismer, M. K.; Reibarkh, M. Facile Quantum Yield Determination via NMR Actinometry. *Org. Lett.* **2018**, 20, 2156–2159. (b) ElMarrouni, A.; Ritts, C. B.; Balsells, J. Silyl-mediated photoredox-catalyzed Giese reaction: addition of non-activated alkyl bromides. *Chem. Sci.* **2018**, 9. 6639–6646.

¹⁵ Graham, M. A.; Noonan, G.; Cherryman, J. H.; Douglas, J. J.; Gonzalez, M.; Jackson, L. V.; Leslie, K.; Liu, Z.; McKinney, D.; Munday, R. H.; Parsons, C. D.; Whittaker, D. T. E.; Zhang, E.; Zhang, J. Development and Proof of

Concept for a Large-Scale Photoredox Additive-Free Minisci Reaction. *Org. Process Res. Dev.* **2021**, 25, 57–67.

¹⁶ Zheng, J.; Swords, W. B.; Jung, H.; Skubi, K. L.; Kidd, J. B.; Meyer, G. J.; Baik, M.–H.; Yoon, T. P. Enantioselective Intermolecular Excited-State Photoreactions Using a Chiral Ir Triplet Sensitizer: Separating Association from Energy Transfer in Asymmetric Photocatalysis. *J. Am. Chem. Soc.* **2019**, 141, 13625–13634.

¹⁷ Genzink, M. J.; Kidd, J. B.; Swords, W. B.; Yoon, T. P. Chiral Photocatalyst Structures in Asymmetric Photochemical Synthesis. *Chem. Rev.* **2021**, *122*, 1654–1716.

¹⁸ Kaphan, D. M.; Brereton, K. R.; Klet, R. C.; Witzke, R. J.; Miller, A. J. M.; Mulfort, K. L.; Delferro, M.; Tiede, D. M. Photocatalytic Transfer Hydrogenation in Water: Insight into Mechanism and Catalyst Speciation. *Organometallics* **2021**, *40*, 1482–1491.

